HET Sky Hex-Burst: A Summary

Prepared by: S. Odewahn
Date: July 28, 2014
Version: 2.0

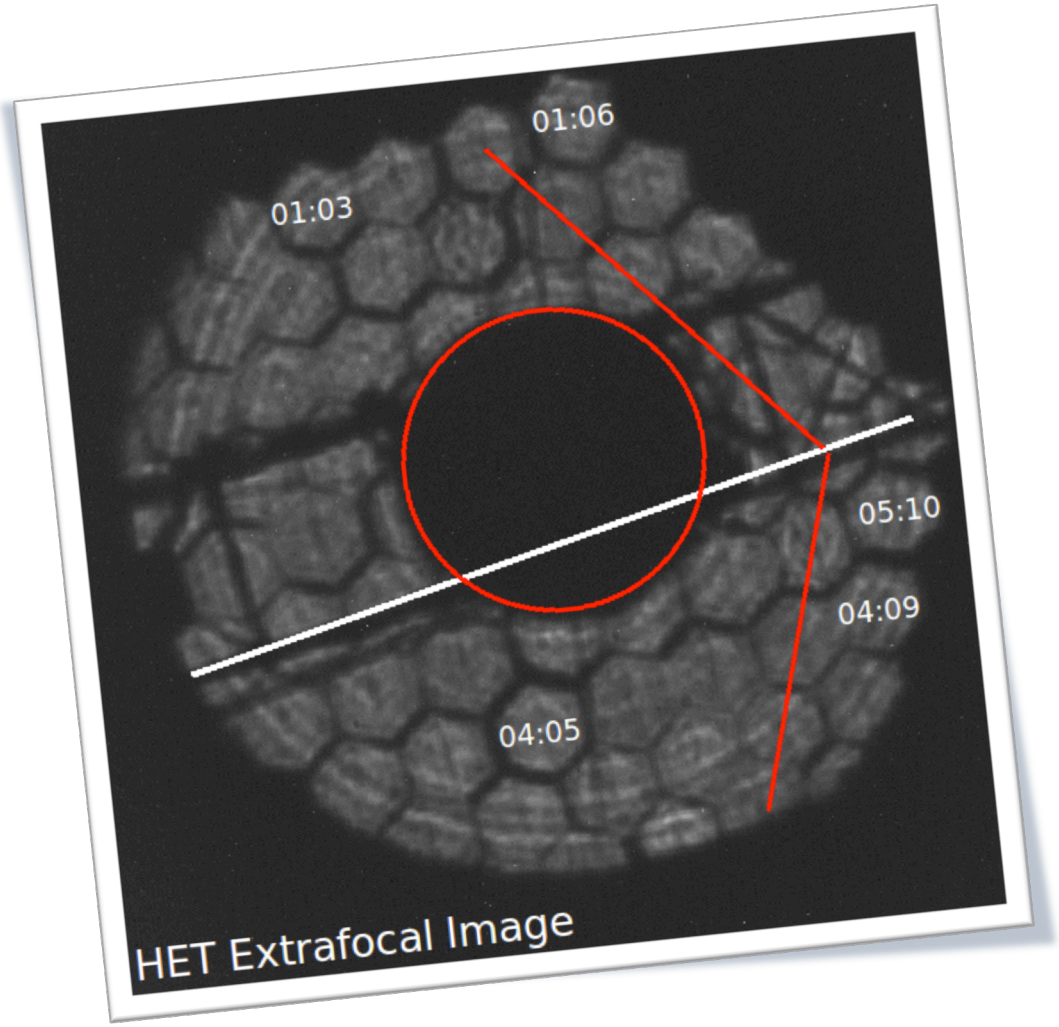

Table of Contents

1 Introduction

The term hex-burst (HB) refers to an engineering procedure used at the HET to assess the relative reflectivity of the mirrors comprising the HET primary mirror, often referred to as M1. A schematic of M1 is shown in Figure 1 with the mirror name designations shown in our two commonly used systems (col:row and single number). The array of 91 mirrors is maintained by the HET mirror group and a major part of the groups activities deal with cleaning and recoating the reflective surfaces of the component mirrors. The HB procedure is used as one means of determining the optimal schedule for mirror recoating. This procedure has been executed in two basic modes:

1. Observations made from CCAS (i.e. from the center of curvature of M1) with the HEFI camera.
2. Observations made of bright stars on sky using the guide camera (FIG = fiber instrument guider).

Each method has its pros and cons. A report evaluating CCAS hex-burst procedures was presented by SCO in October 2011 and the basic result of that work was that irregular illumination of M1 from the CCAS tower made the measurement of mirror reflectivity (particularly for mirrors in the outer area of the array) highly problematic. At that time it was decided that we would return to the practice of conducting a sky HB procedure as often as was practical (at least every other time a major installation of newly coated mirrors was performed).

1.1 Why the cover page figure?

The figure on the cover page of this document, while not that of a hex-burst, conveys a number of key points. The cover image, known as an extra-focal image, is simply an out-of-focus image of a bright star observed with the HET. As such, it represents the exit pupil: that bundle of rays collected by the optical system that reach the focal plane. In essence, we see an image of every part of the collecting area that contributes to the sources viewed in the focal plane. We see the primary (M1) is composed of individual hexagonal mirrors, some of which are partially obscured by shadow or are not full illuminated within the pupil (i.e. they lie outside the illuminated pupil area).

The importance thing to realize from our cover figure is that in any HET image, only a percentage of HET mirrors are fully contributing to the measured total image flux. To perform a measurement of the relative reflectivity of each mirror, we must isolate those mirrors that are fully contributing to the image flux (unless there was some practical way of correcting those mirrors which are only partially contributing). Additionally, the figure illustrates that we must be able to identify mirrors (e.g. the white text labels) that are arranged in a column (e.g. thick white line) and row (thin red lines) pattern. A red circle in the cover figure identifies the spherical aberration corrector (SAC). The SAC and the tracker rails that carry it are the main sources of obscuration (shadow) in the pupil.

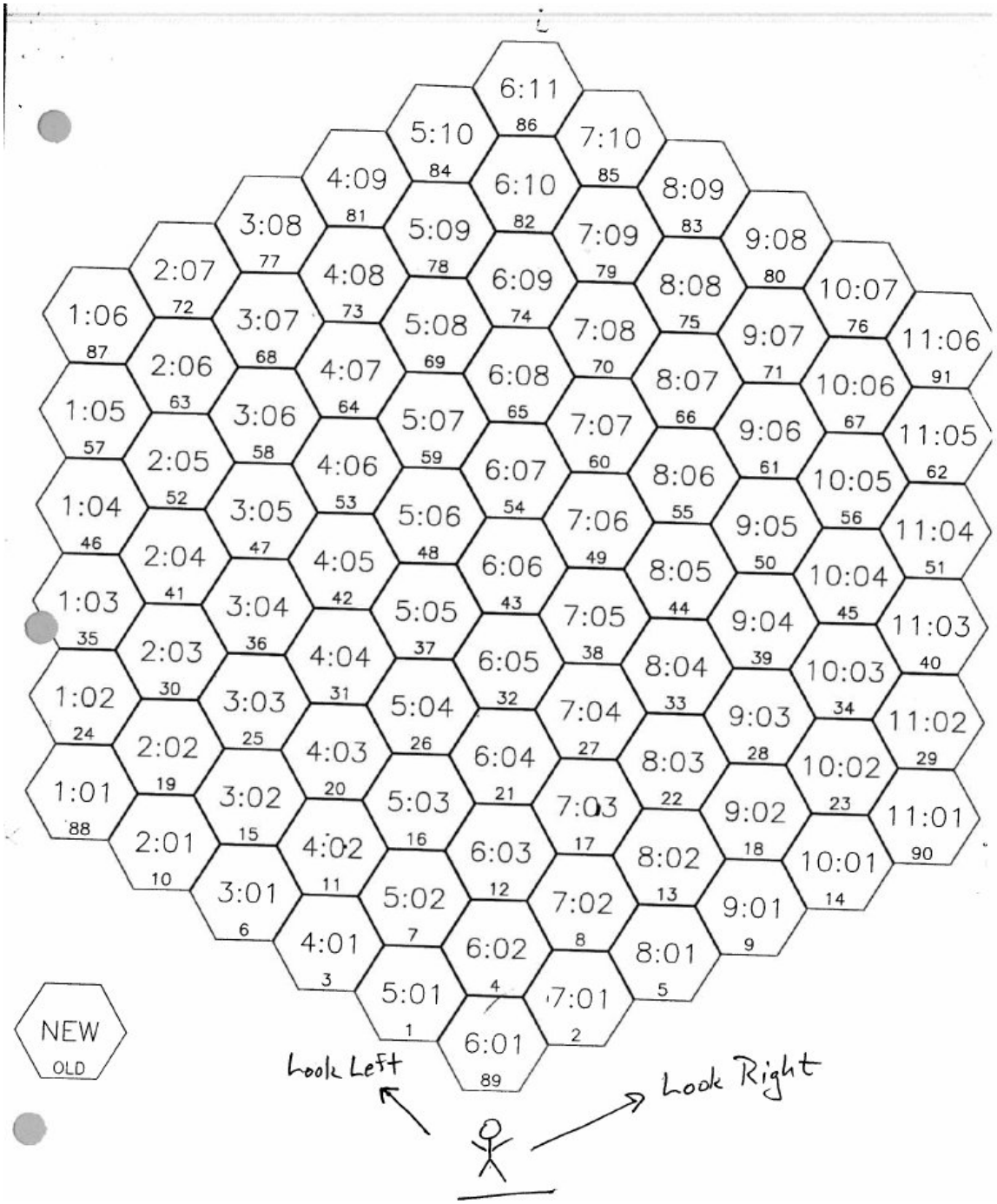

Figure 1: The array of 91 mirrors that form the HET primary (M1).

1.2 What is a hex-burst?

A typical HB image is shown in Figure 2. This is an image from a single bright star. Each component mirror in M1 is supported by three arms. The position of each arm is controlled by an actuator. Hence, the orientation of a component mirror is determined by the settings of the three actuators (designated i,j,k) supporting it. In an ordinary HET image, the component mirrors are oriented such they all register at

the same location in the focal plane (i.e. each image of a point source like a star falls at the same position in the focal plane). With an HB image, the actuators for each component mirror have been adjusted in such a way that its optical axis falls in a unique location in the focal plane. Hence, the HB image allows us to view the stellar image produced by each component mirror of the pupil. This is the essence of the hex-burst procedure. Each stellar source in the HB image is an image of the same star using different mirrors. When we measure the relative brightness of each stellar source in the HB image we are, in turn, measuring the relative reflectivity of these mirrors.

The image in Figure 2 illustrates a number of features of an HET HB image. The pattern of images in a "burst" could be anything, but for convenience, we use a hexagonal pattern that emulates the mirror pattern in M1. Hence, we see a hexagonal array of stellar images. In the coordinate frame of the FIG image columns of mirrors (shown as blue lines in Figure 2) have roughly horizontal orientations. The mirror rows, labeled as red lines in Figure 2, have roughly vertical orientations. The low mirror column numbers are located at the top of the FIG image, and the low mirror row numbers lie to the right side of the FIG image. There are two fundamental steps for analyzing an image like that in Figure 2:

1. We must identify which mirror produces which stellar image
2. We must identify those mirrors which are fully illuminated by the pupil

Having done this, we can integrate the total flux of each identified stellar image and use these measurements to infer the relative reflectivity of each measured mirror.

Figure 2 helps us to realize another important aspect about using HB images. The location of the SAC relative to M1 determines which mirrors will be properly illuminated. The SAC position at the start of a FIG integration are stored in the image header. These values, designated as X_STRT and Y_STRT, are shown in blue text in the lower left corner of Figure 2. These values determine where the SAC shadow (indicated by the red circle) will be located in the HB image relative to the mirror pattern. The actual location of the center of the SAC shadow in the FIG image coordinate frame is finally determined by where the telescope is pointing on the sky at the time of the integration. In short, the job of evaluating the HB image comes down to fitting the pattern of sources so that the image from each mirror is identified, and using the values of X_STRT,Y_STRT to estimate which mirrors are fully illuminated in the pupil at the time the image was taken.

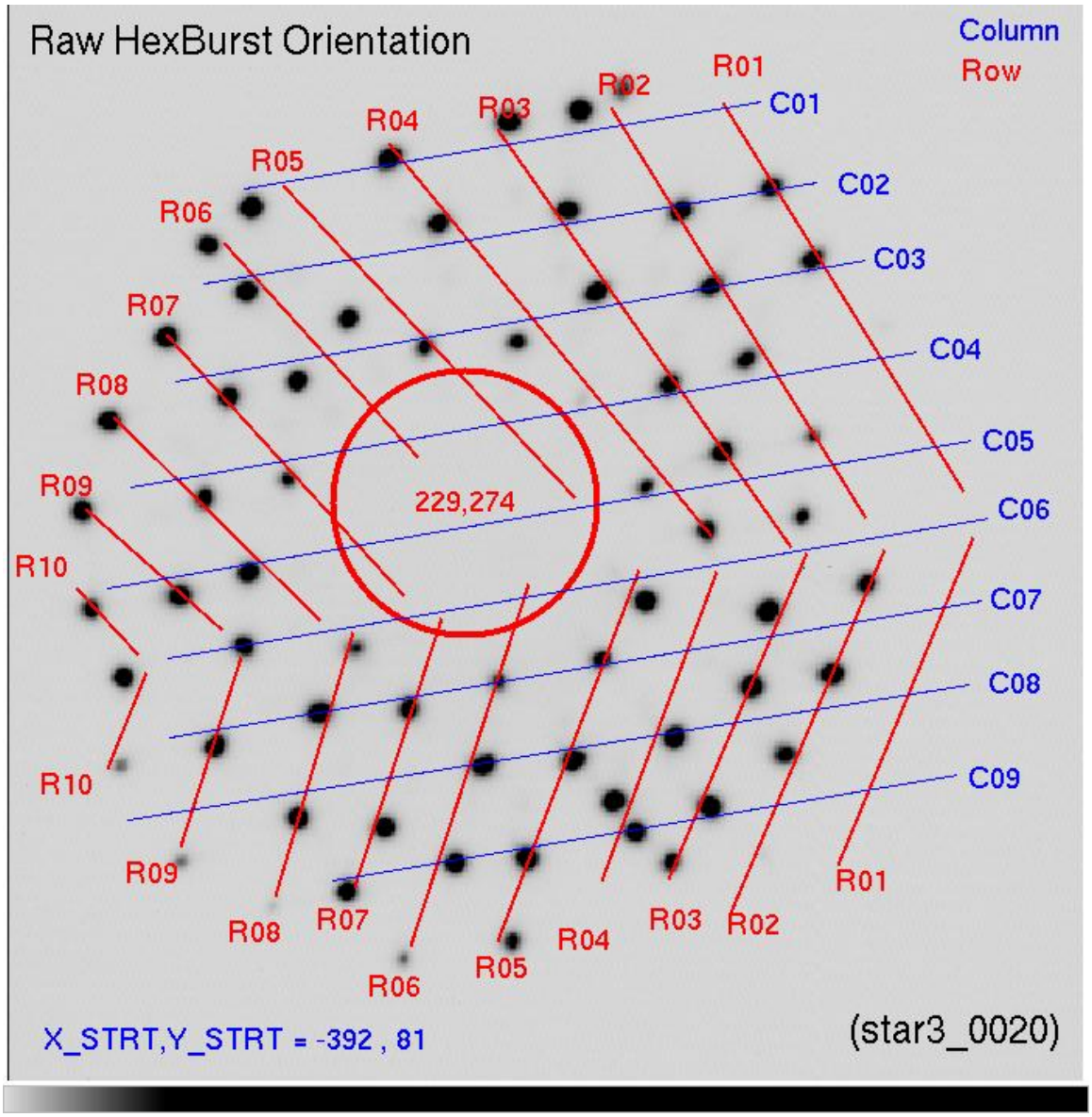

Figure 2: A typical sky hex-burst image obtained with the FIG on HET.

2 Software Tools for Hex-Burst Work

2.1 Fundamental Tools (Primitives)

In the past I have written a number of data pipelines for reducing HB data sets obtained at both CCAS and on sky. These were comprised of more or less monolithic codes that employed a number of routines for performing image display, image processing, and numerical analysis. Because our methodology has changed, we have seen numerous and frequent changes to these pipeline codes. The result is invariably a software nightmare that is difficult to maintain and progressively harder to upgrade. To circumvent this, I have developed a set of rather robust

software tools that work in a stand-alone sense to perform the tasks needed to analyze our CCAS hex-burst data. Briefly, these tools are:

ID (Image Display) – Allows user to display FITS images and record or mark image regions (circle, ellipse, box, text) for various purposes.

MIDO (Measure Image Display Objects) – Performs image analysis according to the type of regions marked in a session with the ID routine.

XYP (XY Plot) – Graphical tool to display results from MIDO and other sources. The user can isolate data points and conduct interactive queries to view supplementary information about a displayed point (i.e. HET mirror identification, mirror photometry, source background value and aperture properties, etc...).

NDF (Numerical Data Fitting) – Executes a variety of numerical analysis tasks using data collected with other tools (primarily with XYP).

2.2 HAT: An Integrated System

From the user's point of view, only one tool is needed to take and reduce HB images: HAT (Hex-burst Analysis Tool). This program invokes all of the above routines to carry the HB observer/reducer through the data reduction and analysis process to the point of creating a list of relative reflectivity for the HET mirrors. All of the reduction steps discussed in the next section are executed with HAT. Any of the critical steps like image photometry or mirror identification can be re-done at any point in the reduction using the fundamental tools (ID,MIDO,...) without re-starting the entire reduction. It is worth noting that there is a secondary level code called HEXFIT. This code can be used via HAT, but also as a stand-alone package, to process both hex-burst and extra-focal images. As the name implies, HEXFIT allows the user to identify a few mirrors directly, or by identifying mirrors rows and columns, and then solving for the global linear transformation that allows one to predict mirror locations in the X,Y coordinate system of the image being processed.

Finally, as will be presented in a following section, the HAT code has a set of tools installed that enable the observer to compose and monitor the data-gathering process at the telescope. In short, for each hex-burst session we normally have a few mirrors that are of primary interest (usually newly installed mirrors). For any desired time, HAT allows the user to select stars from the Yale Bright Star Catalog (YBSC) that will produce optimal measurements of these mirrors. A tally of all

mirrors with valid data, and the number of observations obtained for each, is maintained during the HB observing process.

3 Coordinate Transformations

3.1 What transformations are required?

There are two basic sets of equations and a few parameters that were established for use in gathering and reducing sky HB data. The first, and most important set of equations, relates the position of the tracker (via X_STRT,Y_STRT) from each FIG image header to the position of the SAC shadow in the pupil image. As already explained, this is critical to know since only those mirrors that are unobstructed, and fully illuminated in the pupil image, may be used to measure relative reflectivity. In addition to the SAC position relative to M1, we must know the size of the SAC obstruction, the size of the pupil field, and the size of a single HET mirror in a uniform spatial system. The second set of equations was established to relate the position of a star in the sky (azimuth and altitude) with the position of the tracker (X_STRT,Y_STRT) needed to observe that star. This will also involve the azimuth of the HET structure. In fact, one goal of establishing this coordinate transformation system was to allow the user to adjust the structure azimuth, given an observable star, to optimize mirror observations in particular parts of M1. In the following subsections I review these transformation equations.

3.1.1 A coordinate system for M1

A normalized coordinate system for the array of HET mirrors (M1) was established. This system locates the mirrors in the same hexagonal pattern that the mirrors are positioned in the array. This was used since the SCS (Segment Control System) emulates this same pattern when a HB is performed. The HET normalized units were defined with a center in the middle of M06:06 (see Figure 1). The mirrors M06:11 and M06:01 were defined to have a position of unity in this system. Hence, the linear positions of all other mirrors, designated as $[X_{het}, Y_{het}]$ are determined and the radius of a mirror in this system of coordinates is, by definition, $R_{mirr} = 0.5$. By defining such a system we have, in theory, to use only a spatial zeropoint (x_o, y_o), a scale (M1 normal units per FIG image pixel), and a rotation angle, θ, to convert the HET normalized mirror positions to the coordinate system of any FIG HB image. As explained in the next section, the job of deriving this transformation (i.e. FIG system to M1 system) is performed with the HEXFIT tool. Once a HEXFIT solution was obtained, we could use each extra-focal image to predict, in HET normalized mirror (M1) units, the SAC position, $[X_{het}, Y_{het}]$, the radius of the SAC shadow, R_{SAC}, and the radius of the outer pupil, R_{pup}. It should be noted that the SAC and outer pupil shape were found to have roughly the same center. The outer pupil

extent, defined by a stop somewhere in the SAC system, was found to be slightly non-circular in some cases, but we assume a perfect circle for the work here. Using a set of 15 extra-focal images obtained between 2009 and 2013, we derived values of $R_{SAC} = 0.3465$ and $R_{pup} = 0.8662$ (where we have by definition set $R_{mirr} = 0.5$).

3.1.2 Where is the SAC relative to M1?

The position of the HET tracker is given, for the start of the observation, in every FIG FITS image header via the X_STRT and Y_STRT keywords. In the remainder of the equations of this document these tracker coordinates will be referred to as $[X_{STRT}, Y_{STRT}]$. Since most HB integration times are usually just a few seconds, these values were adopted as the tracker position during the entire image observation. A full transformation of these coordinates to a corresponding position in the pupil image will of course require a spherical trigonometric solution. However, using a simple set of linear equations, it was found that an adequate transformation solution could be empirically derived using a collection of extra-focal images taken with the tracker in a variety of position. For every extra-focal image gathered in this exercise, the ID routine was used to visually mark the size and location of the SAC shadow. In addition, when possible, the outer boundary of the circular extent of the outer pupil image was fit with a circle. As described in the previous subsection, these measurements were used to establish the sizes of the pupil perimeter, the SAC shadow, and an HET mirror in the normalized M1 coordinate system.

Using the 15 sets of measured SAC center positions, $[X_{het}, Y_{het}]$, and corresponding tracker positions from the FIG image headers $[X_{STRT}, Y_{STRT}]$, we derived the following simple linearly independent transformation equations:

$$X_{het} = a1\, X_{STRT} + a2$$
$$Y_{het} = b1\, Y_{STRT} + b2$$

$$a1 = 0.00046 \pm 0.00001 \quad a2 = -0.00223 \pm 0.00124$$
$$b1 = 0.00040 \pm 0.00001 \quad b2 = +0.01293 \pm 0.00017$$

It should be noted that the r.m.s scatter in these solutions indicated a mean spatial uncertainty of about $0.005 R_{SAC}$ in both the X and Y directions (i.e. a 0.5% error in terms of the size of the SAC shadow radius).

An application of this equation set, along with the derived SAC and pupil sizes, is shown in Figure 3. The extra-focal image of Figure 3 has been processed with HEXFIT to predict the locations of valid (i.e. fully illuminated) mirrors for hex-burst analysis. The locations of the SAC shadow and outer pupil perimeter are shown as red circles. The locations of valid mirrors are indicated with cyan circles, and the mirror identifications are labeled. As can be seen in Figure 3, the selected mirrors lie well within the pupil perimeter and well outside the SAC shadow. One caveat is that the area between the tracker rails (the horizontal linear shadows in Figure 3) are

filled with obstructing struts and cables. Hence, for reflectivity measurements, no mirrors located inside the two tracker rails are selected for use by the HAT software system. In fact, one might question whether M05:02 in Figure 3 is being slightly obstructed by a cable shadow just below the SAC. This is probably a shadow caused by the HRS/MRS fiber cables. This was never a significant problem in the past, but in the future *a pupil image containing the VIRUS IFU cables and support arms may indeed cause substantial complications*.

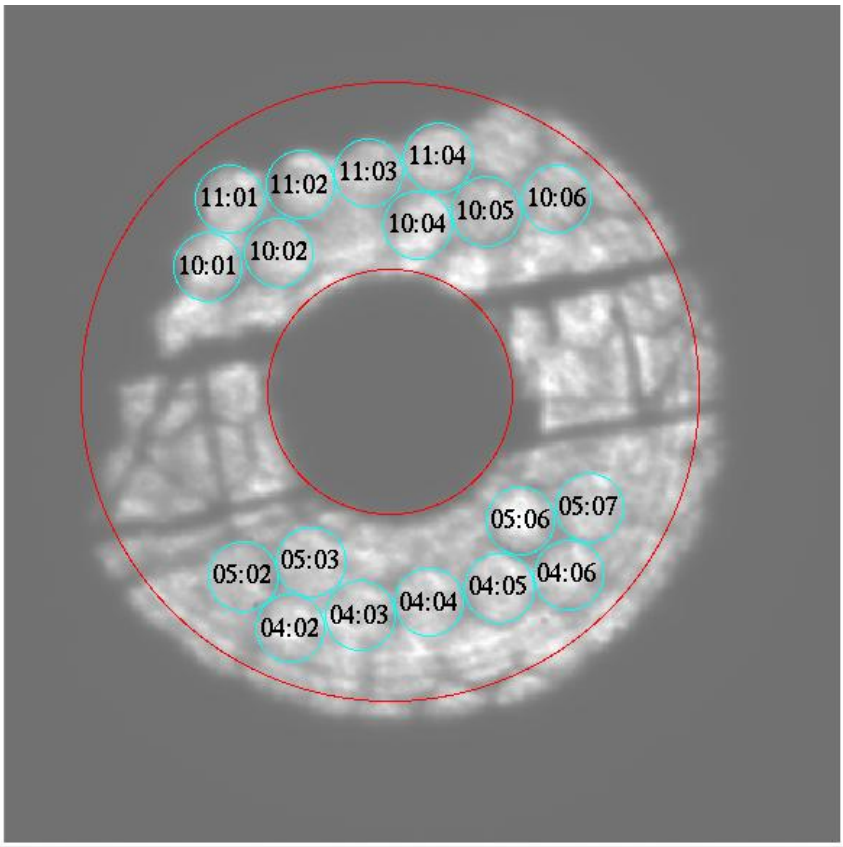

Figure 3: An extra-focal image with well-illuminated M1 mirrors marked by the HEXFIT package.

3.1.3 What stars are observable?

In order to cover M1 with as many mirror measurements as possible in a set of HB data we must select a variety of stars that will distribute the values of $[X_{het}, Y_{het}]$ over a wide range. Also, it was desired that we have measurements made of newly installed mirrors as soon as possible. Hence, a method was established by which stars were selected on the sky to insure the observations of sets of HET mirrors during the HB data collection process. As discussed earlier, the YBSC was used to select stars with a sufficiently bright U magnitude (generally $U \leq 8.0$) so that high S/N images were recorded with a FIG integration time of 5-10 seconds using the UV filter (n.b. this is really a U filter, but the name UV is used in the FIG gui and using

anything other than the name "UV filter" frequently proved problematic). In practice we specify a UT time for when each observation was to be made. The azimuth and altitude, $[AZ, ALT]$, were computed for every YBSC star for that UT. Of these stars, all those located outside the HET annulus (a 10^o wide annulus with a central radius located 55^o from the zenith) were excluded. For each remaining star the tracker position, $[X_{STRT}, Y_{STRT}]$ was predicted via the equations:

$$X_1 = 60.0\ (AZ - AZ_S)\cos(ALT)$$

$$Y_1 = 60.0\ (ALT - 55°)$$

$$X_{STRT} = c1\ X_1 + c2$$
$$Y_{STRT} = d1\ Y_2 + d2$$

$c1 = \ \ 3.6291\ \pm 0.0001 \quad c2 = \ \ 0.315\ \pm 0.013 \quad \sigma_x = \ \ 2.89\ mm \quad N = 6256$
$d1 = -3.6284 \pm 0.00001 \quad d2 = -22.520 \pm 0.013 \quad \sigma_y = 13.52\ mm \quad N = 5815$

The values of the (c_1, c_2, d_1, d_2) coefficients were derived empirically using the header information in large numbers (given by N above) of archival LRS images. The LRS image headers contained all of the information needed to evaluate the above coordinate sets (i.e. HET structure azimuth, AZ_S, time of observation, UT, sky position, $[\alpha, \delta]$, and corresponding tracker coordinates, $[X_{STRT}, Y_{STRT}]$ (in mm units). Once the tracker coordinates of each star were computed, then the list of fully illuminated mirrors for each star could be computed using the numerical recipe described in the previous section.

In practice, the above equation set was used to compute the complete track of each YBSC star selected in this manner. A plot of the track, such as that shown in Figure 4, could be made so that the observer could judge the direction of the track across M1 and which mirrors might be observed by prolonging the time of observation. The green circles in Figure 4 represent track position prior to the requested UT and the red circles represent track position after the requested UT. The coordinates in Figure 4 are in the normalized HET mirror system (i.e. these are $[X_{het}, Y_{het}]$) and the positions of mirrors in M1 are labeled in purple text.

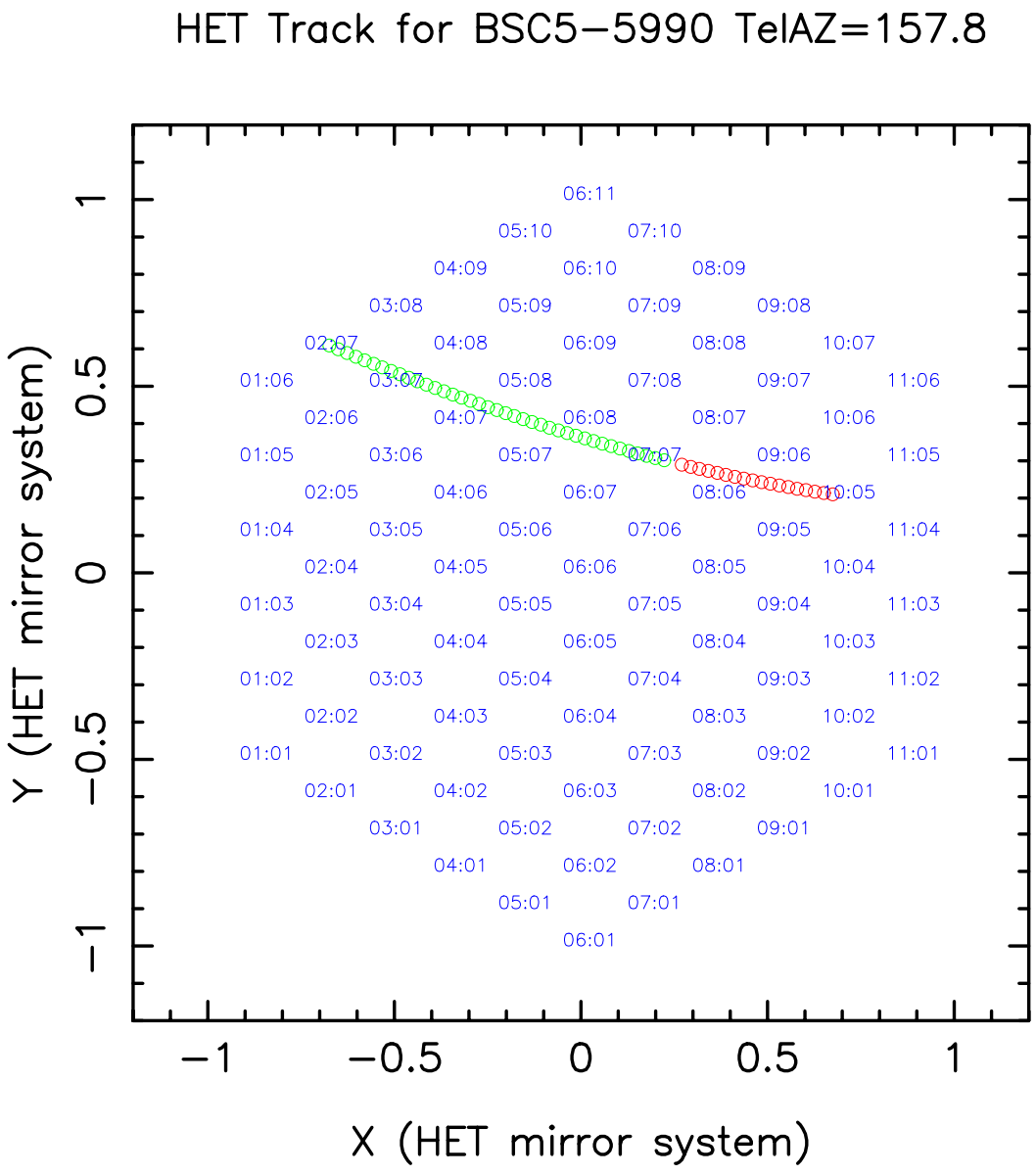

Figure 4 A sample HET track figure. Green points are the start of the track.

4 Obtaining sky hex-burst data at the HET

The HAT software package presents an option (sky hex tools) at the start of each run that allows the user to select lists of potential stars for HB observations. The observer can select stars based on desired area of the sky or even the mirror which is deemed most desirable for observation (i.e. one of the newly installed mirrors). As described previously, a chart of the HET track, like that displayed in Figure 4, can be displayed in interactive form. The user may click on any of the green or red circular points to determine the UT time that the star will be positioned so that the tracker is at that point in the M1 reference frame. Moreover, as a set of HB observations progress, HAT produces a file named "observed_mirrors.out" that will summarize, for each HET mirror, how many observations of fully illuminated mirrors have been made.

4.1 The TO/RA procedures

The procedures that the telescope operator (TO) and resident astronomer (RA) perform when HB data are gathered are summarized in the following list. At the time this document was prepared (Dec2013) the HET was undergoing a comprehensive hardware and software upgrade. Many of the procedures below will be outdated. However, a number of procedures will remain valid, and some of the tasks will be updated to suit the new systems when operations resume. Finally, this list (compiled by V. Riley) can serve as useful historical documentation of how the HB observing procedures were executed at the time of the take-down in August 2013.

1. Stack
2. Move translide to position 3
3. Insert FIG Luminosity filter
4. Set FIG to 2x2 binning
5. Receive target RA,DEC and structure AZ from RA
6. Acquire target: ttp, focus
7. Place star at X,Y=256,256
8. Insert FIG UV filter
9. SAMS to Standby
10. SCS to manual mode
11. TCS off
12. Apply hhex_bst.smf twice (/home/jove/guider/SCS/move_files)
13. Straightem mirror columns/rows (if needed)
14. Set a SAMS reference
15. SAMS operate (close loop)

16. SCS back to SAMS (close loop)
17. Find integration time that give peak counts near 8000-20000 ADU
18. Autosave images (name synatx hex_star1_0001 and do not forget to set starting number back to 1 for each star). Set to 60s and click Time for the autosave to save 1 image per minute.
19. Apply hhex_com.smf TWICE (/home/jove/guider/SCS/move_files)
20. Load SAMS reference from WHEN YOU STACKED.
21. SAMS Operate (close loop)
22. SCS set back to SAMS (close loop)
23. Insert Luminosity filter
24. Move 10mm out of focus (Focus Offset = +10)
25. Adjust int time to peak adu near 40,000 ADU
26. Save images (Autosave mode in FIG guider, exfoc_star1_0005)
27. 10mm IN focus (return to best focus)
28. Return to Best Azimuth

4.2 Some observing caveats

There are a couple of important things to remember when conducting sky HB observations at the HET. The first is that the CCAS tower can obscure the HET field of view in a variety of positions. In Figure 5 I have compiled a collection of extra-focal images made with bright stars observed with HET structure azimuth positions in the range $45 \leq AZ_s \leq 95$. Clearly, the altitude of the star will also determine where the obscuring shadow of the CCAS tower is located in the pupil image, but avoiding this azimuth range during HB observations will go a long way in avoiding this problem. Of course, some software package that predicts the influence of the CCAS tower should be developed and installed in HAT for future data taking.

A second important point to remember is that the FIG is a CCD camera, and one should acquire flat field images with the filter used for HB observations (UV) for every data set. This was not frequently done in the past, but should have been. In Figure 6 we see a typical (master stacked frame) FIG UV flat field made in a few minutes during sunset. Clearly there are large-scale variations at the level of 10% that could be easily removed with a simple flat-field correction of the HB images prior to reduction.

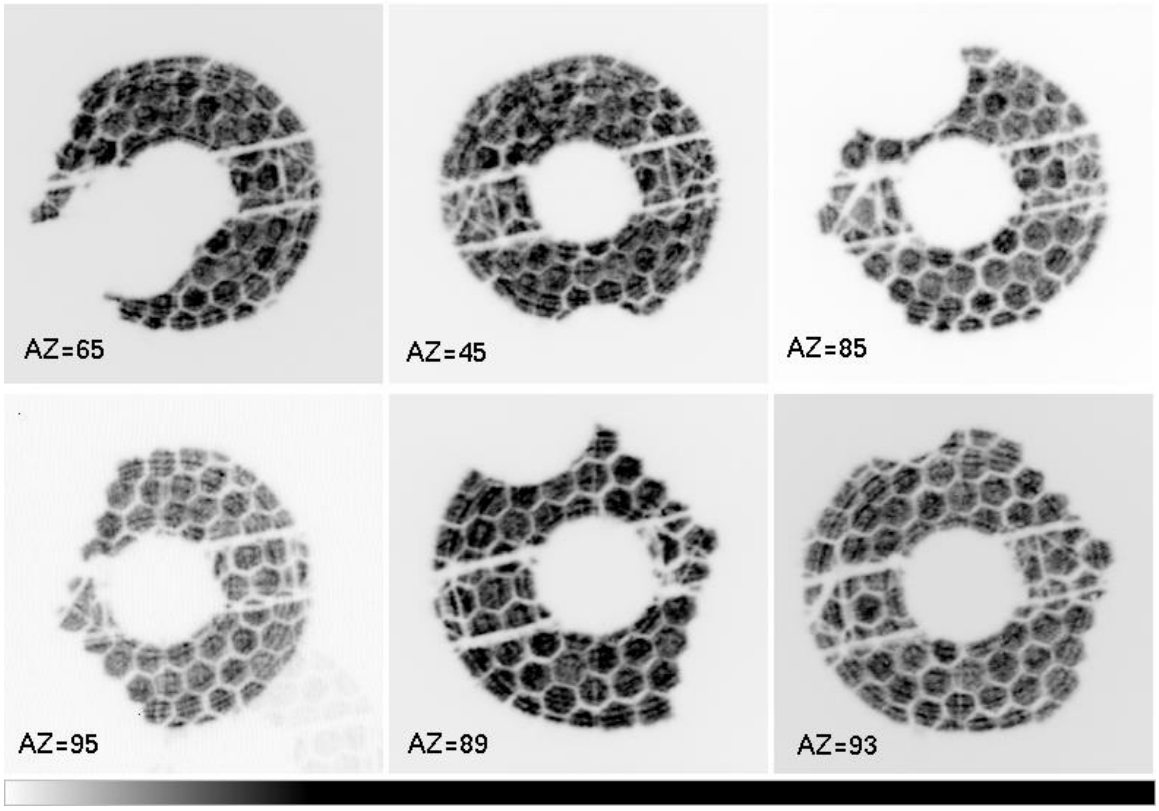

Figure 5: Extra-focal images showing the HET CCAS tower.

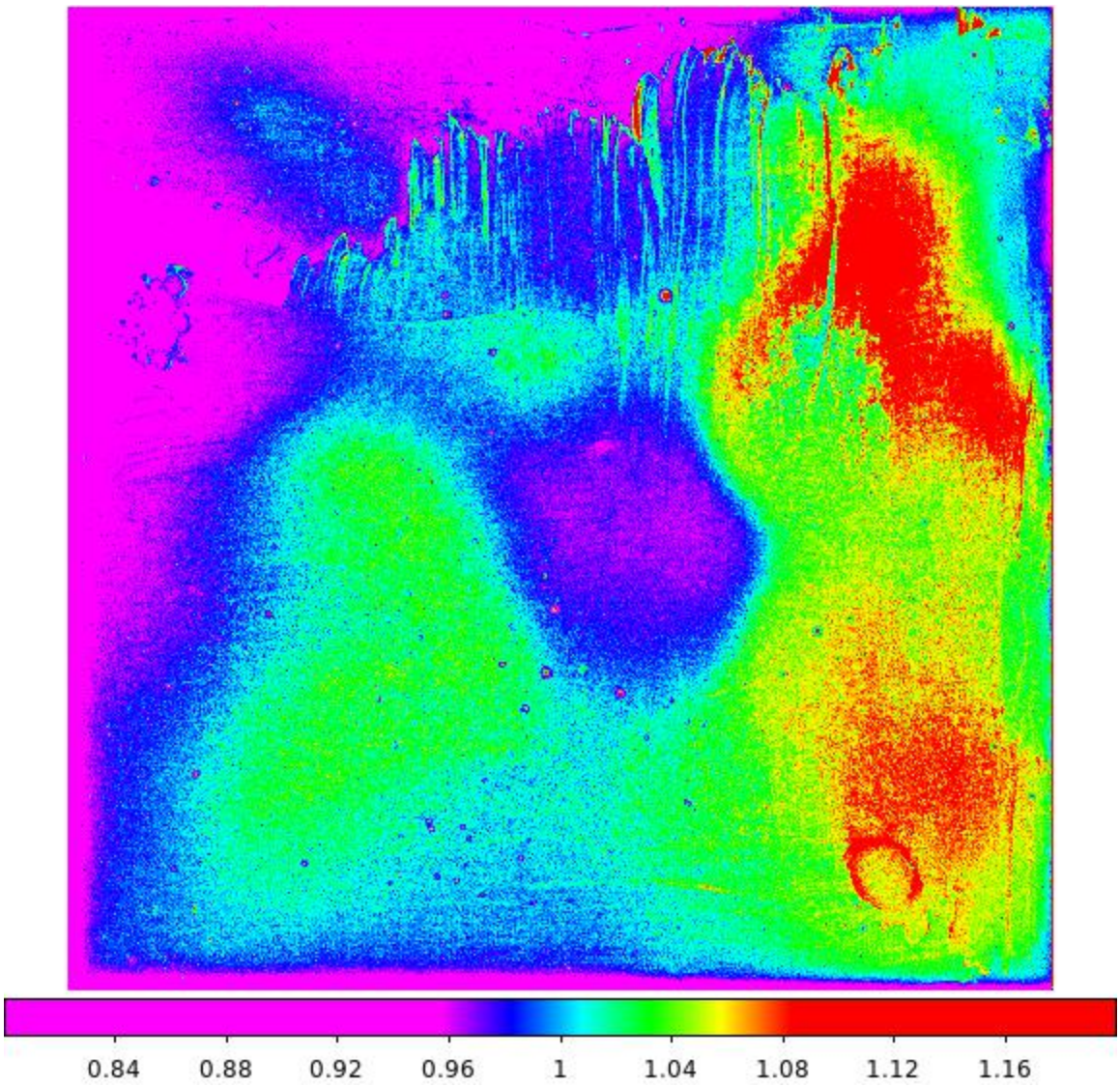

Figure 6: A typical flat field master frame obtained withe UV filter on the FIG.

5 Reducing HB images

The job of reducing sky HB images is completely handled by the HAT package. A significant amount of human interaction is required for various secondary packages discussed in Section 2 of this document, but all of the steps may be run within the HAT domain. The purpose of this section is not to describe every step in the reduction pipeline for processing HB data. These steps invariably change, and there are existing web-based documents that describe at some level these steps. Rather, this document will give a high-level overview of the process.

5.1 Basic reduction setup

The directory structure for the HB data will have been established during the data taking phase. We typically will have a main directory with the name of the hex-burst date (e.g. 20130222) and in that location we'll have sub-directories for each star observed with names like Star1, Star2, etc. Finally, I create a sub-directory named "files" that contains important information for the particular HB set in question. The most basic file is "Basic.info" which contains things about the date of the mirror replacements, the mirrors replaced, and the name of the HB data set. A second file (usually with a name like "Swap.Log_20130222") will also reside in /files. This file, constructed from the Excel file sent by Logan Schoolcraft for every HB session, contains information about the mirror coating dates and the types of coatings applied. Rather than cover the formats of these files in any detail here, it is suggested that the interested reader view the files in the (ghex) directories for HB directories that are maintained by Odewahn on mcs, banzai, and buckaroo. When the directory structure is properly built, I typically perform the following:

1. Run gethead to view the INSFILTE values in each image header to insure that the UV filter was always used for the FIG images.
2. I run the HAT book keeping and special reduction initialization setup.

5.2 Mirror identification in the HB images

As described in the previous section, a normalized cartesian coordinate system has been established that describes the mirror positioning in M1. The most basic task to be performed for every HB images is to derive the transformation that converts X,Y values in pixel coordinates in the image system to this normalized system. With this transformation we can begin to identify the mirror images present in each HB image. The first section of data reductions in HAT (and by far the most time consuming for the user) is the running of HEXFIT on each image to derive this coordinate transformation solution. For each image HB image, the reduction sequence is as follows:

1. The user specifies which image file is to be processed.
2. The user identifies a few representative mirror images. These are then used as template PSF images to find all remaining mirrors in the HB image (using the sparse PSF sampling method).
3. Using the ID routine (via HEXFIT) the user (a) identifies a few mirror directly or (b) identifies mirror rows and columns.
4. Using the X,Y image positions of all PSF sources from step 2, and the mirror identifications from step 3, a least squares fit is performed to derive the transformation equations needed to transform image X,Y to $[X_{het}, Y_{het}]$. This solution is used to identify all possible mirrors.
5. Using the method outlines in Section 3, all well illuminated HET are established and aperture photometry for each source is performed.

For every HB image processed in this way, a finding chart such as that shown in Figure 7 is produced. In such a chart, all identified in this step (whether properly illuminated or not) are over-plotted with mirror names in the HB image. The image name is listed bottom center, and the tracker position, $[X_{STRT}, Y_{STRT}]$, is shown in the upper right.

5.3 FCOMBINER: Transformation to a uniform photometric system

After the individual mirrors on each HB image have been identified and their photometry (brightness) has been measured the final step in our reduction process is to combine all of the valid measurements for each mirror and produce a combined final list of mirror relative reflectivity values. The job might appear to be simple at this point: for each mirror we collect all magnitude estimates from the measured images and compute a mean estimate of the magnitude (i.e. the brightness). These mean magnitudes are then converted, via a logarithmic inversion, to a reflectivity scale using a zero-point that is set at some level, in our case the level defined by the brightest mirror image (i.e. the brightest mirror is defined to have a reflectivity level of $R = 1$). As with nearly all things hex-burst, this apparent simplicity does not hold.

The fundamental problem we are faced with in combining all of the hex-burst measurements is that each HB has its own photometric system. With each mirror image having a total integrated flux, T_f, we compute a magnitude:

$$m = C - 2.5 \log T_f$$

Our complication derives from the fact that the value of C is image dependent, even for a fixed FIG integration time. This variation in C may be small for a few HB images taken within a small time window on a photometric night. However, it is more often the case that HB engineering is performed on nights of poor science condition (i.e. far from photometric) and hence each image may be obtained under varying observing conditions (e.g. varying cloudy cover, wind speed, and seeing). Moreover, in the course of developing a pipeline for processing HB data, it was discovered that there exists a large systematic effect with distance of a measured mirror from the center of the SAC shadow center.

5.3.1 Mean ZP determinations

In the case of most HB data sets, each star is observed 10-15 times: 1-5 sec integrations are taken once every 60sec for some period. Hence, the positions and illumination of the HET mirrors in the resultant HB images do not change a great deal, but the conditions under which they are taken can change (i.e. the value of C may change). To correct for this, we cross-match the mirror set for each hex-burst image with some master set to find the number of common mirror measurements between the pair. This cross-matched set will normally consist of a dozen or so well illuminated mirrors. The residuals between these magnitudes ($r = m_i - m_M$) are

used to compute a mean zero-point correction, C_i, for each image, i, in the set of images for a star. The question of how to define the primary set, M, is problematic. In our case we simply cross-matched every set of mirrors from each image in a set with all other mirror lists for the set. That image which produced the largest number of cross-matches was selected to define the mean zero-point, C_M, for that set of images. Hence, a mean residual, $< r >$, was computed using all mirrors in image i that were common to the master system, M. These mean residuals were used to compute the zero-point, C_i for each HB image. In a second pass, all image-dependent zero-points were applied, and common sets of magnitudes, now in a uniform photometric system, were computed. For each set of mean magnitudes a brightest magnitude was selected, as described above, and a set of relative reflectivity values, R, were computed for all measured mirrors.

5.3.2 De-trending with SAC radius

After the above step, it was anticipated that combining photometry from different stars, to create a plot of mirror reflectivity, R, verses coating age, A, would be straight forward. In many cases this was so, and our plots of reflectivity against age produced very smooth relations with the expected trend: older coatings have lower reflectivity. However, it was frequently found that many such plots produced a disturbingly large number of outlier points.

In the course of researching the source of these discrepant points we discovered a significant trend in the HB photometry. The measured brightness of a mirror measurement depended on the distance of that mirror from the center of the SAC shadow. An example, made with observations from two stars in a single HB data set, is shown in Figure 8. As discussed above, our plots of reflectivity verse coating age often revealed discrepant points. To track the origin of these occurrences, we fitted a simple linear regression to the entire set of $[R, A]$ points from any HB reduction set. Relative to this linear regression fit we computed residuals for each mirror and plotted these as a function of numerous quantities used in the reduction. The important result from this approach was found in a plot, like that of Figure 8, of reflectivity residual verses SAC radius, R_{SAC}. A statistically significant slope, measured at better than the 5σ level, was found separately in 4 different HB reductions (each set being comprised of 3-7 stars measured on about 50-70 images). The solutions for the slope of this trend were combined and the following relation was established to remove this systematic trend from our reflectivity measurements:

$$\Delta_R = 1.0 + g_2 (R_{SAC} - g_1)$$

where $g_2 = 0.6$ and $g_2 = 0.599$

It should be noted that the value of g_1 was selected to represent the mid range of the R_{SAC} values found in most data sets. The value of g_2 was computed using an unweighted mean of 4 derivations from different HB data set reductions.

Using the de-trending expression above, the final FCOMBINER plots of $[R, A]$ from HAT, such as shown in Figure 9, were largely free of discrepant outlier points. In the end, such outliers were found to be real (e.g. a poorly coated M05:06 returned to the array to study the aging of a bad Al coating).

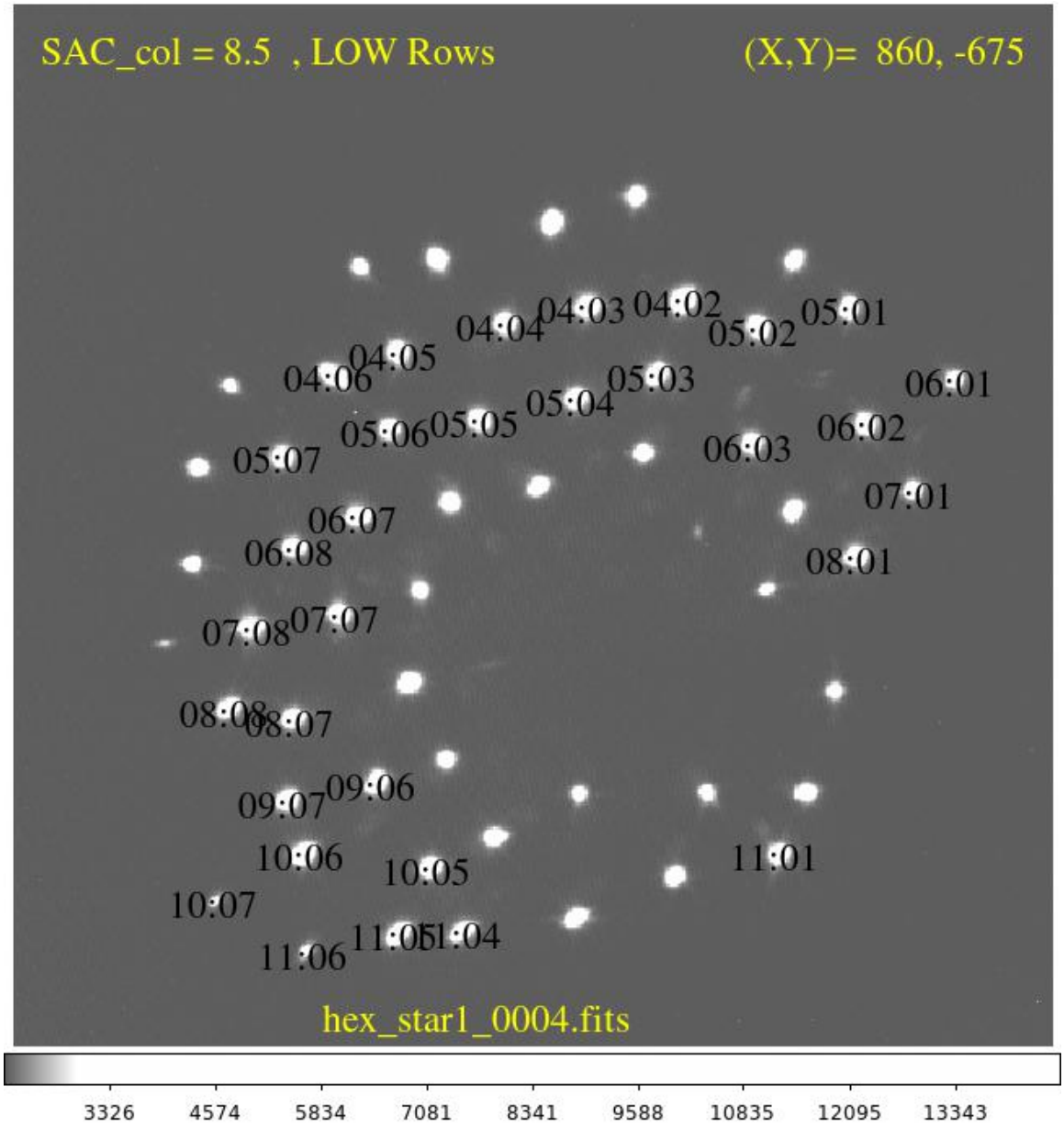

Figure 7: A hex-burst image processed with HEXFIT.

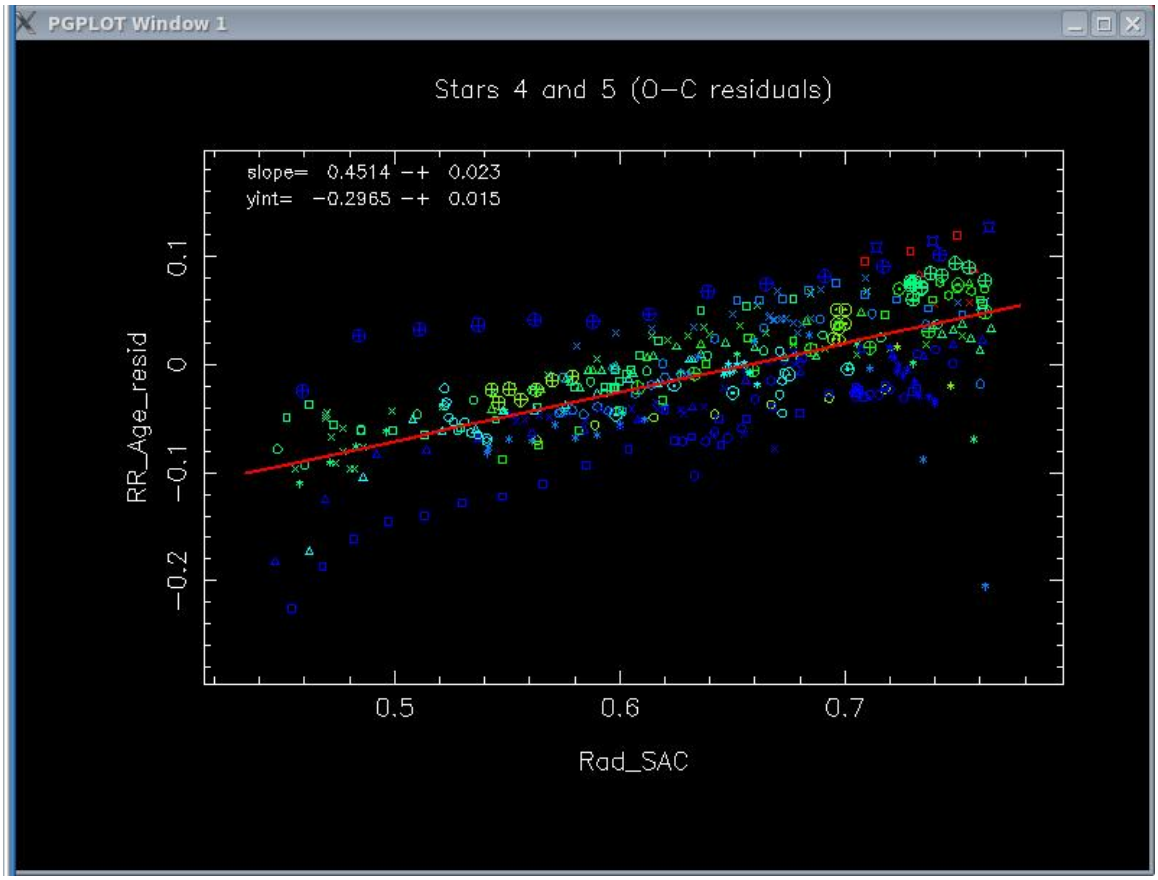

Figure 8: The trend in mirror reflectivity as a function of distance from the center of the SAC shadow.

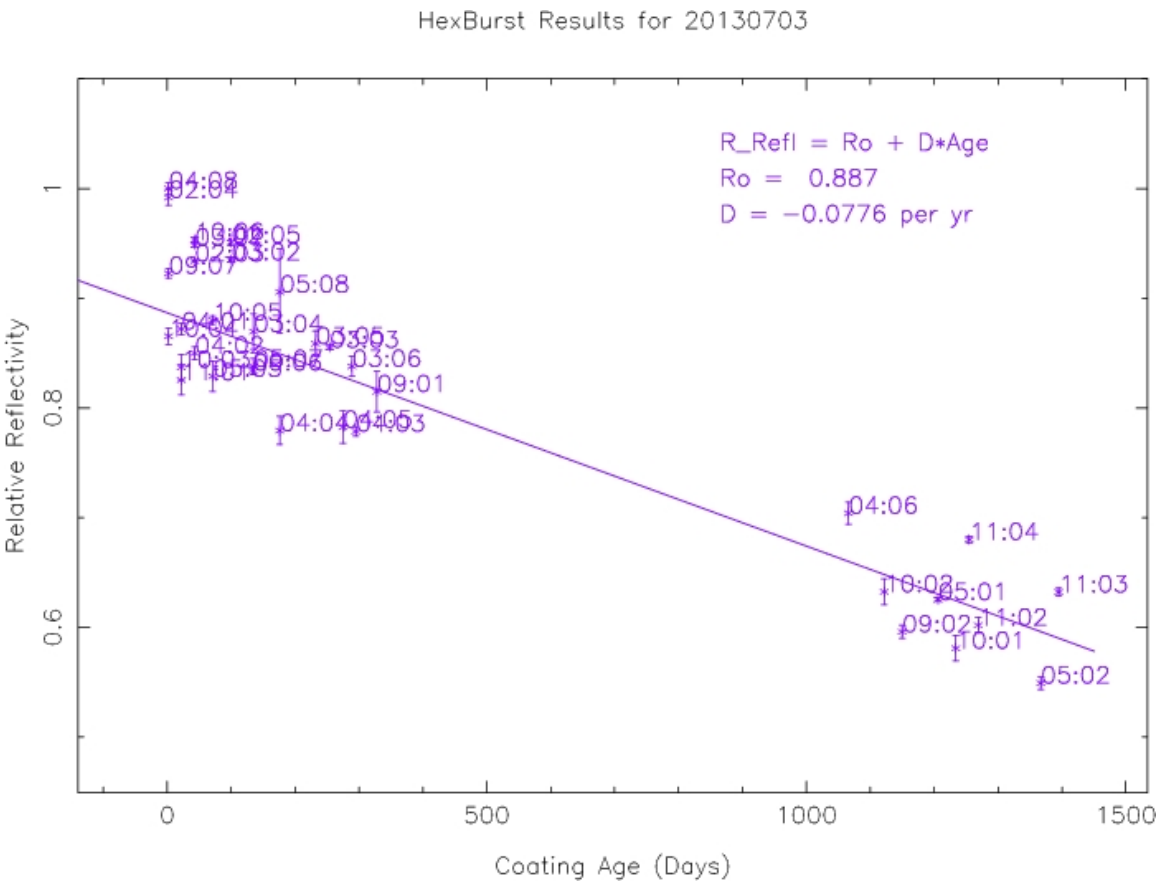

Figure 9: The final result of a HB data set reduction.

6 Reflectivity by Coating Type

6.1 Available Data

A total of 4 sky hex-burst data sets that were observed between Feb2013 and Jul2013 were assembled. As explained in a previous section, the primary product of a sky HB exercise are lists of mirror relative reflectivity, transformed to a uniform photometric system, using observations of 5 to 10 bright stars (in the U filter with the FIG camera). Each mirror in the resulting data set has a coating type and an age for that coating at the time of the observations. The photometry is normalized such that each hex-burst set yields a relative reflectivity of $R = 0.92$ for a coating of age zero. This level was assigned on the basis of a 92% reflectivity being the anticipated reflectivity of a newly coated aluminum mirror. In this section, we break the hex-burst data sets into 5 distinct coating types and conduct an analysis that will address the rate of degradation in coating reflectivity, as well as the relative degree of reflectivity between coating types. The coating group names, the number of available mirrors with data, $\boldsymbol{N_m}$, and information about the minimum, maximum and mean ages of the coatings in each group are summarized in Table 1. We also list

the number of original and final (not rejected at the 2.5σ level) points used in the analysis of each coating type in Table 1.

It should be mentioned that the coating group referred to as OTHER represents a collection of several coating types and methods. No single member of the OTHER group yielded a set of data adequate for analysis, and hence the entire set (comprising 6 mirrors) was collected into one *catch-all* group.

Table 1: Coating age information

Coating	N_m	A_{min}	A_{max}	$< A >$	A_{wid}	N_s	N_f
107Al	54	0.633	4.356	3.227	1359	127	125
BareAl	24	0	1.074	0.479	392	71	68
Al+SIO	21	0	0.636	0.183	232	52	52
Al+PDIB	5	0.329	0.899	0.655	208	19	19
OTHER	6	0.115	0.868	0.552	275	21	21

6.2 Method of Analysis

The photometry of the individual hex-burst images, having been transformed to a uniform photometric system, can be compared to yield relative reflectivity measurements of the primary mirrors. Each hex-burst set, if normalized to a system where the brightest mirror is assigned a relative reflectivity of 1.0, may be compared directly with other such sets. The idea is that the most reflective mirrors will be represented by the newest and presumably most highly reflective coatings. Since for every mirror in each collected data set has a coating age (in years) and a relative reflectivity in some a system, we can study the degradation of reflectivity with time. Since we have a collection of hex-burst data sets for mirrors having different coating types, we can hope to quantify the rate of reflectivity degradation with time for each coating surface.

The collected hex-burst data, namely relative reflectivity, R, and coating age, A, were grouped by coating type. For each collection of data, we fit a linear regression of the form:

$$R = \alpha A + R_o$$

where the slope, α, is the degradation rate in fractional decrease per unit time, and the intercept, R_o, is the relative reflectivity for a mirror with a new coating (zero age). As the HB method is purely differential in nature, the measured α values are the most meaningful, but since each data set is comprised of different coating types, the derived R_o values can also provide some information about the intrinsic reflectivity of different coating types. We fit linear regressions for a set of 5 distinct coating types present in the HET primary mirror between Feb2013 and Jul2013. All available data were collected for each type of coating. Values of $[\alpha, R_o]$ were derived for each coating type set. The data, especially for some coatings having few points and small age ranges, were sometimes noisy. To assess the role of discrepant points,

values of $[\alpha, R_o]$ were tabulated using 3 different methods. Each method is briefly summarized in the following subsections.

6.2.1 Method 1 –Direct linear regression fit

In the first approach (Method 1) we simply fit a linear regression to all points. One cycle of 2.5σ rejection was used to eliminate outliers. The standard deviation of residuals (in the Y=Age axis) and the linear correlation coefficient were tabulated for each fit.

6.2.2 Method 2 – Fit to binned points

The points in each coating set were binned in four equal-sized bins in age (the X axis). In each bin a median reflectivity, R, was computed. The median reflectivity computed in this way is more robust to the influence of outlier points. In all five coating cases, we used 4 bins. The final binned points were fitted with a single linear regression (no rejection iterations).

6.2.3 Method 3 – Weighted means of single mirror fits

All data available for each coating type were collected into single mirror sets. For example, all BareAl coatings were collected for mirror 04:06, and the resultant set of points were fit with the same linear regression form of our basic fitting equation. In this case, a minimum number of 4 points was required for such a fit (one measurement per HB data set was required). The resultant sets of $[\alpha, R_o]$ values, and there estimated errors, were collected for each coating set. Weight values for each fit parameter were predicted as $w = {}^{1}/_{me^2}$, where me is the mean error estimated for each fitted parameter in the least squares fit. A weighted mean value was then computed for each parameter in the $[\alpha, R_o]$ sets. Additionally, the median $[\alpha, R_o]$ values were computed and compared to the weighted mean estimates to detect cases of substantial disagreement. Using the 4 Feb-Jul HB sets analyzed here we found good agreement between mean and median estimates for all coating cases.

The available data for each coating type, and the fits derived form methods 1 and 2 are shown in Figures 1 through 5. The Method 1 lines are represented by thin red lines, and cover the full range of each X (age) axis. In these plots for individual coating types we hold the Y (reflectivity) plot range fixed, but the X range (age) is adjusted for the range available in each data set. Rejected data points are encased in black squares. For the Method 2 fits, we display the binned (median) values as large point symbols, with each having a 1.0σ error bar plotted (the standard deviation about each mean point was used here). The linear fit to these median points are plotted as lines extending only over the age-range of the binned points. For each Method 2 line, the color of the line is the same as the color used to plot the original mirror measurements. As can be seen in Figure 10-14, the two methods give results that agree well.

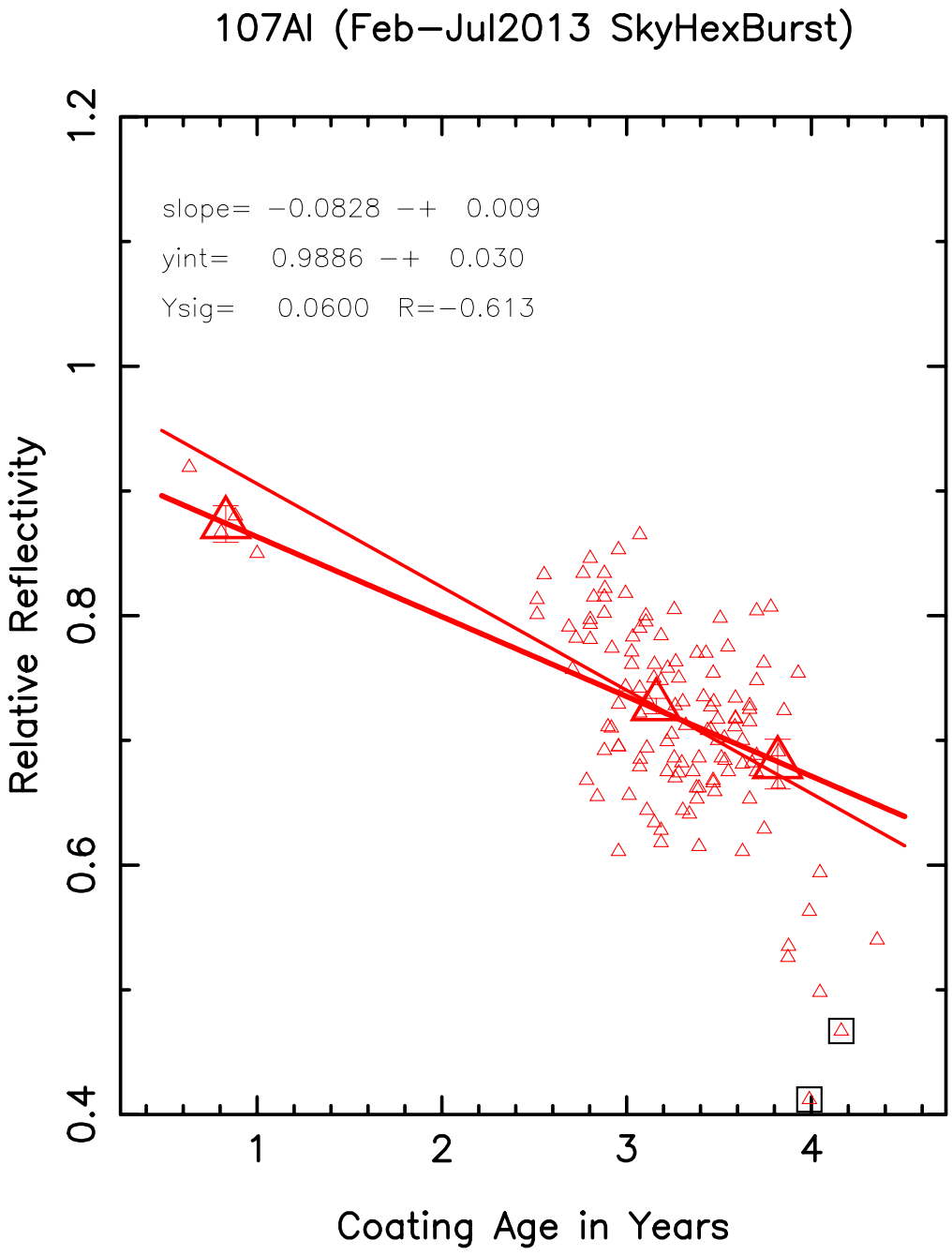

Figure 10: Reflectivity vs. age fits to the 107Al data.

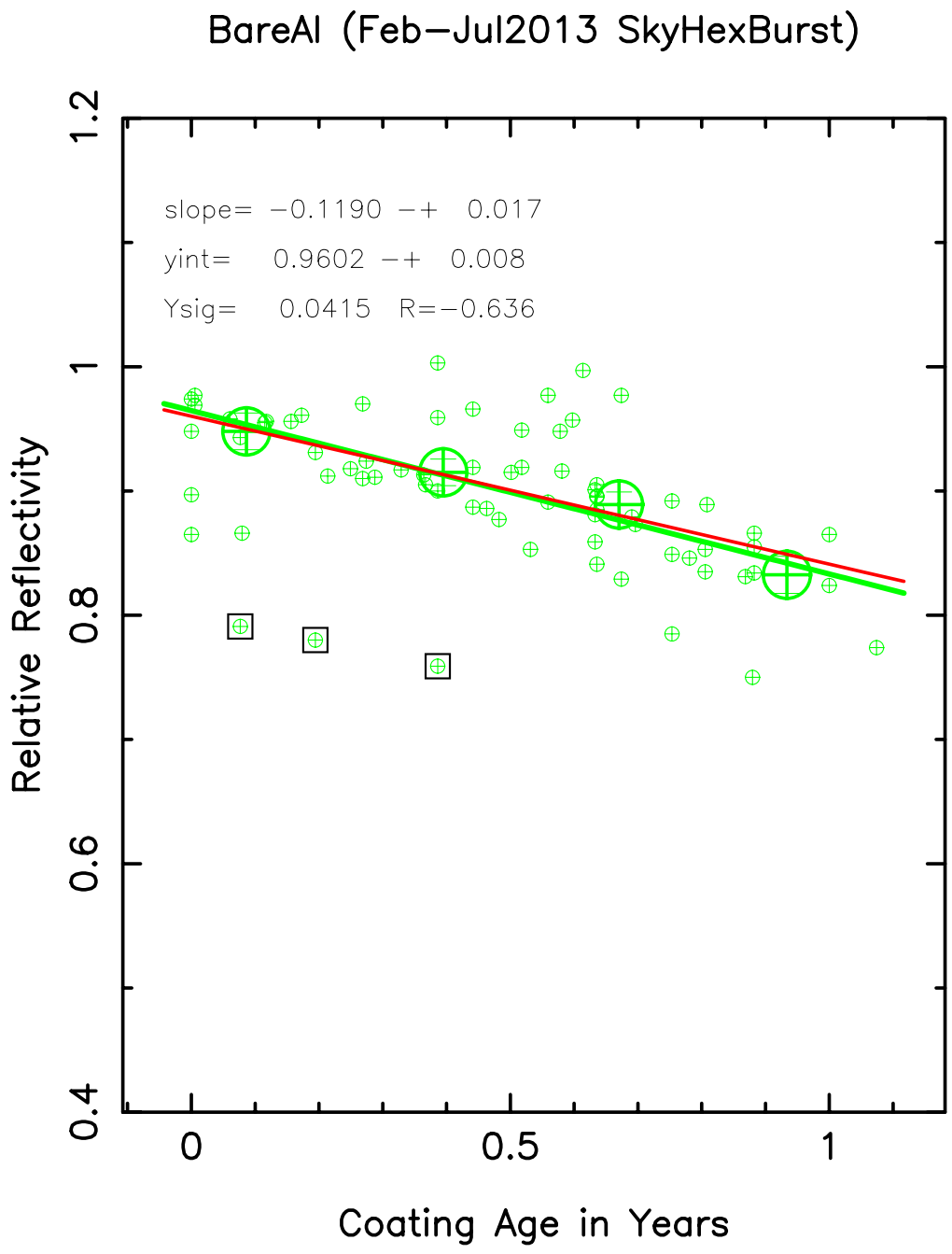

Figure 11: Reflectivity vs. age for the BareAl data.

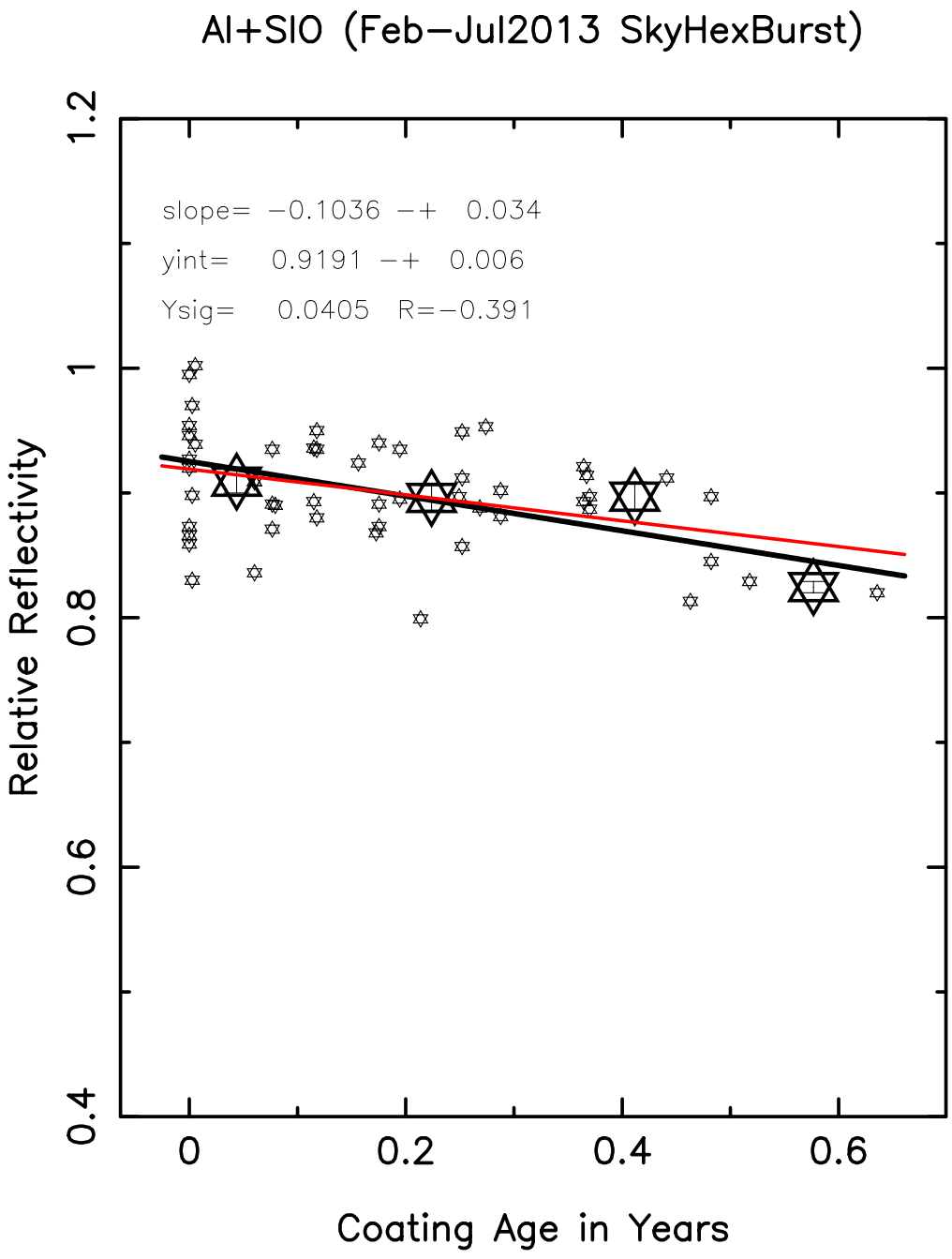

Figure 12: Reflectivity vs. age fits for the Al+SIO data.

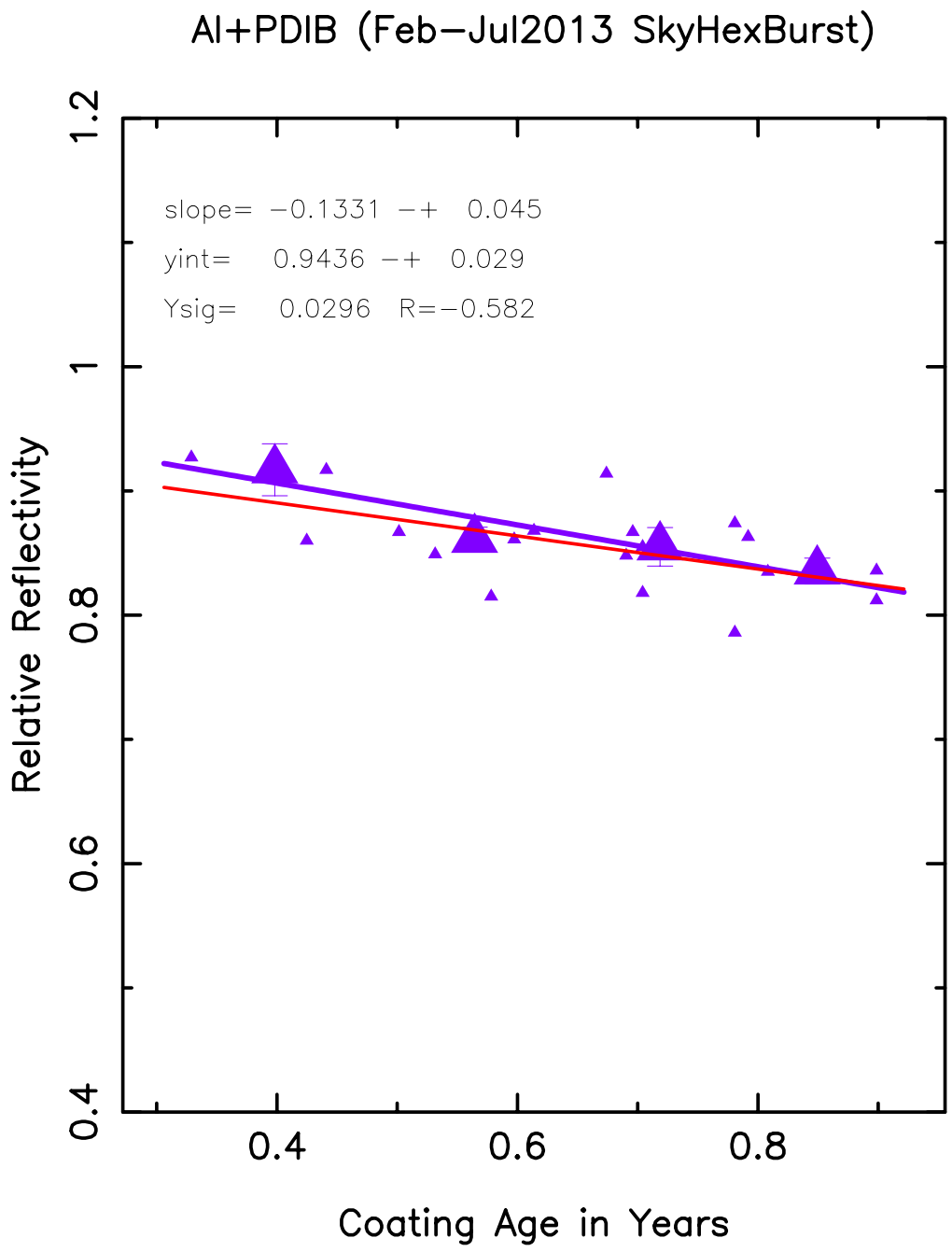

Figure 13: Reflectivity vs. age fits for the Al+PDIB data.

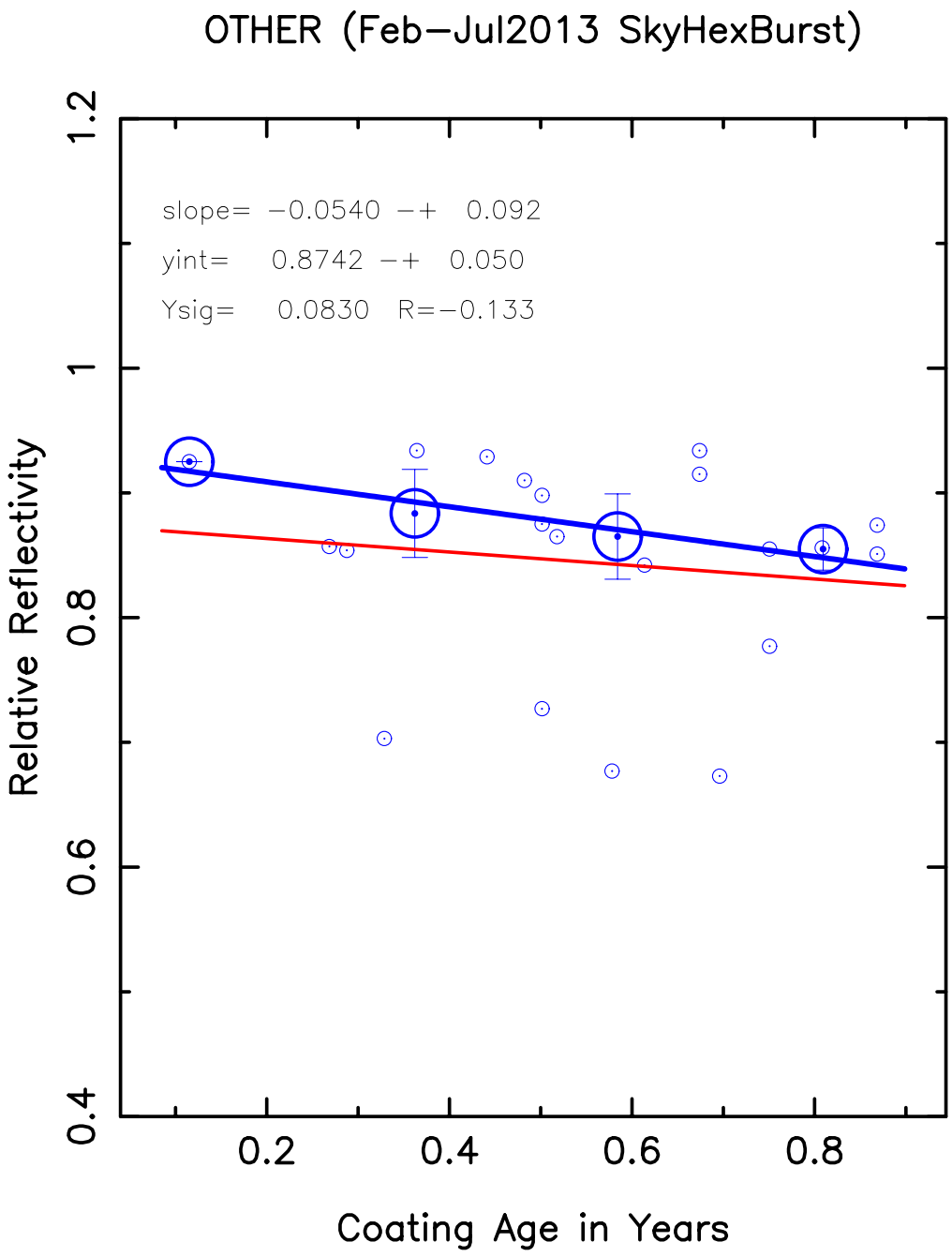

Figure 14: Reflectivity vs. age fits for the OTHER data.

6.3 Summary of Results

In Figure 15 we plot all of the data in a single figure along with the linear fits from Methods 1 and 2 from each coating type. From this single plot one can judge the relative ranges of age available for each coating set, as well as the relative reflectivity degradation (slope) and relative mean reflectivity (Y intercept). The $[\alpha, R_o]$ values and their estimated mean errors from each of the three methods are listed in Table 2. Where appropriate we list the 1σ residual scatter ($\boldsymbol{\sigma_Y}$) and the linear correlation coefficient ($\boldsymbol{R_{corr}}$) for each derivation. The initial and final (after 2.5σ rejection) numbers of points are also tabulated for each coating type and analysis method.

Table 2: Summary of parameter derivations

$\boldsymbol{\alpha}$	$\boldsymbol{me_\alpha}$	$\boldsymbol{R_o}$	$\boldsymbol{me_{R_o}}$	$\boldsymbol{\sigma_Y}$	$\boldsymbol{R_{corr}}$	$\boldsymbol{N_s}$	$\boldsymbol{N_f}$	coat	method
-0.083	0.01	0.989	0.031	0.06	-0.614	127	125	107Al	1
-0.064	0.001	0.927	0.004	0.003	-1	3	3	107Al	2
-0.083	0.016	0.982	0.039	0.125	NA	10	NA	107Al	3
-0.119	0.018	0.96	0.009	0.041	-0.637	71	68	BareAl	1
-0.131	0.019	0.965	0.01	0.009	-0.98	4	4	BareAl	2
-0.104	0.041	0.961	0.021	0.069	NA	11	NA	BareAl	3
-0.103	0.034	0.919	0.006	0.04	-0.39	52	52	Al+SIO	1
-0.139	0.065	0.925	0.021	0.021	-0.832	4	4	Al+SIO	2
-0.009	0.053	0.892	0.015	0.038	NA	6	NA	Al+SIO	3
-0.133	0.045	0.944	0.03	0.03	-0.583	19	19	Al+PDIB	1
-0.168	0.044	0.973	0.028	0.012	-0.937	4	4	Al+PDIB	2
-0.18	0.054	0.984	0.034	0.069	NA	4	NA	Al+PDIB	3
-0.053	0.092	0.874	0.051	0.083	-0.132	21	21	OTHER	1
-0.1	0.02	0.929	0.009	0.008	-0.961	4	4	OTHER	2
-0.083	0.021	0.841	0.05	0.1	NA	4	NA	OTHER	3

As can be seen in columns 1 and 3 of Table 2, the $[\alpha, R_o]$ from each of the 3 method generally agree with one another within the estimated errors. It should be noted that the 107Al set has a significantly larger age span than the other coating groups due to a recoating of a single mirror (08:04) in July 2012, after the HET mirror coating facility was active. It is evident from the figures in this section that the shorter age span (including 107Al sans 08:04) seems to produce steeper degradation rates compared to the 6% to 8% (per year) degradation rate of the full 107Al group. The BareAl, Al+SIO, and Al+PDIB groups seem to yield reflectivity degradation rates in the 10% (per year) or greater range. The one other fairly robust result is that the Al+SIO zero age reflectivity (R_o) is consistently down by 3%

to 5% compared to the other coating groups. A quick review of Table 1 reveals that the mean age of the Al+SIO group is significantly lower than the other coating groups, and hence any firm conclusions regarding the effectiveness of SiO overcoats should be deferred to a time when more data, spread over a larger time range, can be analyzed.

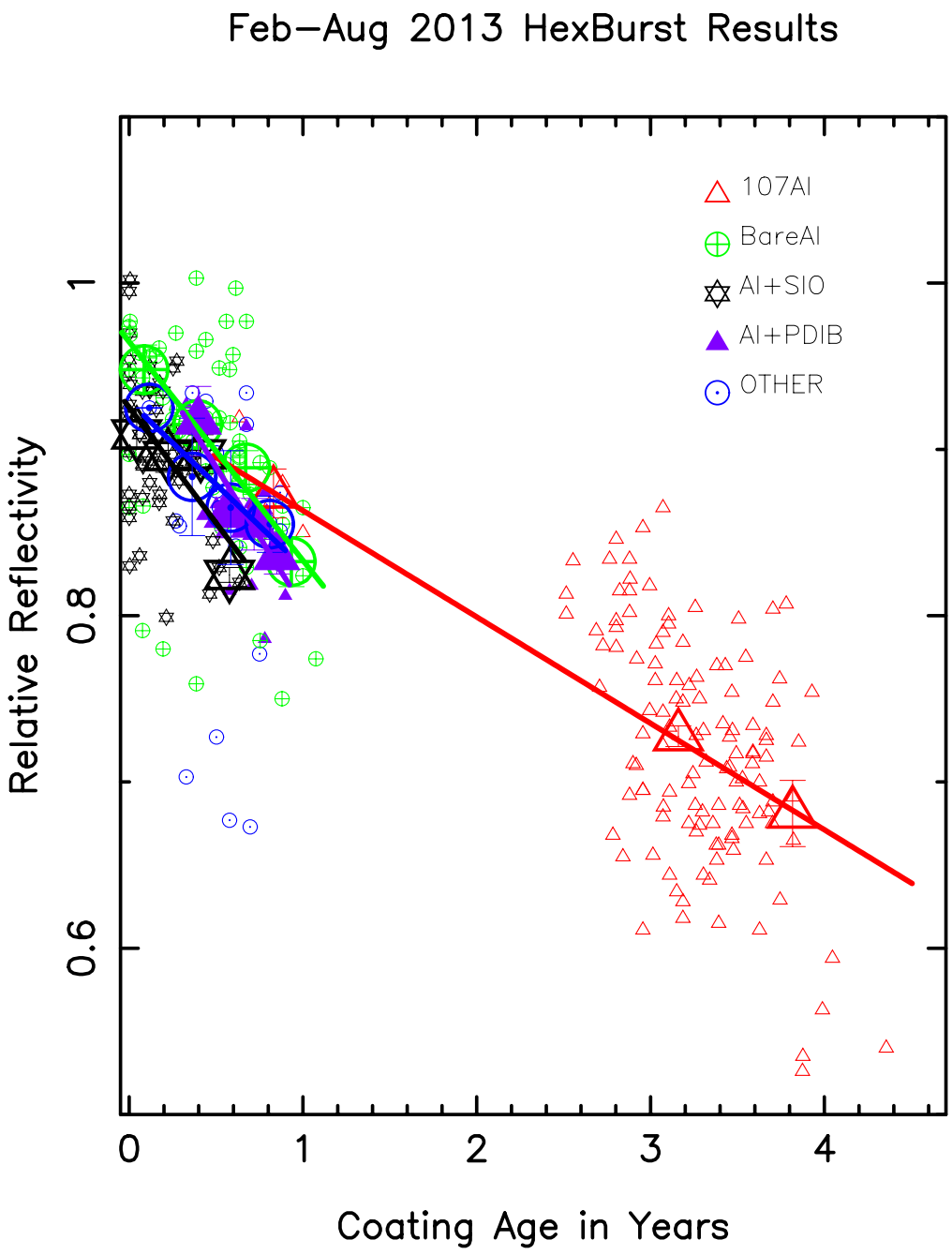

Figure 15: All fit data available in the current coating type analysis.

7 Suggestions for future work.

In the course of this work a number of points have arisen that suggest changes to the HB data gathering process that will surely improve the quality of these measurement.

1. Every HB date set should have at least one set of UV filter sky flats collected.
2. Some dedicated engineering time should be used to collect extra-focal images of bright stars that systematically cover the range of tracker X,Y used in HET observations. This will allow a more comprehensive mapping of the pupil illumination as well as predictions of when the CCAS tower will interfere with observations.
3. We should revive efforts to perform HB observations at CCAS. This will require a dedicated instrument that has a stronger light source that provides even illumination of M1, and a more appropriately selected CCD camera for collecting images. The CCAS method will require less science (sky) time to be used, but more importantly, will provide more strongly controlled and reproducible data gathering. Using a CCAS approach we should be able to accurately map the pupil (via extra-focal images) for every tracker position used to collect hex-burst images. Hence, we will establish a much reliable list of well-illuminated HET mirrors in this exercise.
4. A higher level of data collection automation should be established. The degree of human (bot TO and RA) interaction required to collect the data discussed here is prohibitive. Given a software platform that both takes the images, and communicates mirror adjustments to SCS, one can envision the collection of HB images with extremely well ordered mirror patterns that are collected in a significantly shorter time period.